

RESEARCH ARTICLE | NOVEMBER 12 2024

Nonlinear conductivity of aqueous electrolytes: Beyond the first Wien effect

Hélène Berthoumieux ; Vincent Démery  ; Anthony C. Maggs 



J. Chem. Phys. 161, 184504 (2024)
<https://doi.org/10.1063/5.0226773>



View
Online



Export
Citation

Articles You May Be Interested In

KoopmanLab: Machine learning for solving complex physics equations

APL Mach. Learn. (September 2023)

Experimental realization of a quantum classification: Bell state measurement via machine learning

APL Mach. Learn. (September 2023)

Nonlinear conductivity of aqueous electrolytes: Beyond the first Wien effect

Cite as: J. Chem. Phys. 161, 184504 (2024); doi: 10.1063/5.0226773

Submitted: 3 July 2024 • Accepted: 24 October 2024 •

Published Online: 12 November 2024



View Online



Export Citation



CrossMark

Hélène Berthoumieux,^{1,a)} Vincent Démery,^{1,2,b)} and Anthony C. Maggs^{1,c)}

AFFILIATIONS

¹ UMR CNRS Gulliver 7083, ESPCI Paris, PSL Research University, 75005 Paris, France

² Univ Lyon, ENSL, CNRS, Laboratoire de Physique, F-69342 Lyon, France

^{a)} Electronic mail: helene.berthoumieux@espci.fr

^{b)} Author to whom correspondence should be addressed: vincent.demery@espci.psl.eu

^{c)} Electronic mail: anthony.maggs@espci.fr

ABSTRACT

The conductivity of strong electrolytes increases under high electric fields, a nonlinear response known as the first Wien effect. Here, using molecular dynamics simulations, we show that this increase is almost suppressed in moderately concentrated aqueous electrolytes due to the alignment of the water molecules by the electric field. As a consequence of this alignment, the permittivity of water decreases and becomes anisotropic, an effect that can be measured in simulations and reproduced by a model of water molecules as dipoles. We incorporate the resulting anisotropic interactions between the ions into a stochastic density field theory and calculate ionic correlations as well as corrections to the Nernst–Einstein conductivity, which are in qualitative agreement with the numerical simulations.

Published under an exclusive license by AIP Publishing. <https://doi.org/10.1063/5.0226773>

I. INTRODUCTION

Almost a century ago, Wien probed the response of strong electrolytes under very high electric fields, up to 0.05 V nm^{-1} . He demonstrated a generic increase in the conductivity upon increasing the electric field and later found an increase for weak electrolytes; these two phenomena are the first and second Wien effects.¹ The first Wien effect was explained by Wilson² and later Onsager and Kim, who extended the Debye–Hückel–Onsager (DHO) theory^{3,4} to finite electric fields.⁵ According to the DHO theory, ions are surrounded by a cloud of counterions, which is distorted under an external electric field. This distorted cloud generates an additional drag on the ions and reduces their mobility, thereby reducing the conductivity of the solution. Wilson, Onsager, and Kim showed that large electric fields destroy the ionic cloud, thus restoring the bare mobility of the ions, which leads to an increase in the conductivity compared to the small field limit. The second Wien effect, which was explained by Onsager, is due to the increase in the dissociation constant of a weak electrolyte under a large electric field.⁶ At present, fields of up to 0.1 V nm^{-1} are routinely applied in nanofluidic devices involving atomically thin membranes,^{7,8} electrodes,⁹ or channels.¹⁰ Such high fields gave experimental access to the second Wien effect for water dissociation⁸ and are also used for the investigation of other

ionic transport phenomena, including the ionic Coulomb blockade⁷ or the creation of ion-based memristors in confined geometries.^{10,11} These experiments call for a better theoretical understanding of the behavior of electrolytes under large electric fields.

Recently, the response of strong aqueous electrolytes has been investigated using classical molecular dynamics (MD) simulations with an explicit description of water.^{12,13} Unexpectedly, the conductivity was found to be a constant function of the electrostatic field, up to electric fields of 1 V nm^{-1} . Applying the electric field to the ions only and not to the water molecules, a large increase in the conductivity has been recovered.^{12,13} These results suggest that the molecular properties of water also affect the nonlinear response of electrolytes. However, most of the theoretical efforts from the DHO theory, such as its recent reformulation using Stochastic Density Field Theory (SDFT) and its extensions^{14–20} or approaches based on the mean spherical approximation,²¹ have focused on a better description of the ions, leaving aside the molecular properties of the solvent. The external field polarizes water by aligning the dipoles of water molecules (Fig. 1) and affects two important water properties for ion transport, making them anisotropic: its permittivity^{22–25} and its viscosity.^{26–29} Classical MD simulations report that even at high field strengths of 1 V nm^{-1} , the increase in

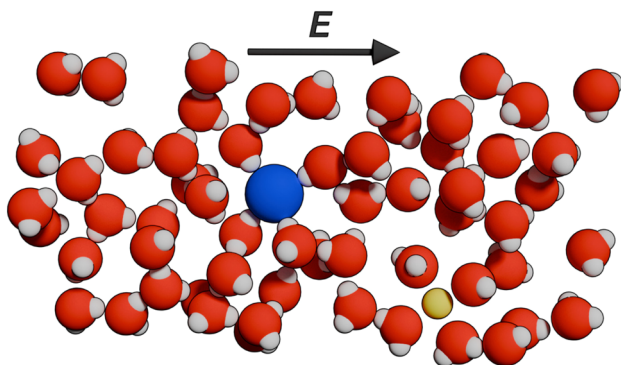


FIG. 1. Snapshot of the classical MD simulations with an electric field of 0.5 V nm^{-1} . The sodium and chloride ions are represented by a yellow and blue sphere, respectively. The orientation of the water molecules by the external field (black arrow) is clearly visible.

viscosity remains moderate²⁹ while the permittivity decreases by an order of magnitude.²⁴

Here, we show that the field-induced decrease in water permittivity leads to an increase in ion–ion interactions and compensates for the Debye cloud deconstructuring. In addition, we find that for a certain range of electrostatic fields and electrolyte concentrations, the cloud enhancement effect induced by the permittivity drop is dominant, resulting in a decreasing conductivity. We use a model of water as dipoles on a lattice^{22,30} to encode the molecular properties of water in a field-dependent, anisotropic permittivity tensor. We then incorporate this permittivity tensor into SDFT to obtain the ionic correlations and the conductivity of the solution, which is nonmonotonic in the electric field. We show that the nonlinear response is controlled by the interplay of two characteristic electric fields: the electric field E_c , where the ionic cloud is destroyed for a constant permittivity, and the electric field E_w , needed to orient the water molecules. Finally, while the main effect is due to the permittivity drop, the permittivity anisotropy significantly affects the conductivity.

II. CONDUCTIVITY FROM MOLECULAR DYNAMICS SIMULATIONS

We ran classical molecular dynamics simulations to measure the conductivity of aqueous solutions of NaCl using the rigid, non-polarizable SPC/E model for water^{31–33} at moderate concentrations $\rho = 75$ and 150 mM and at temperature $T = 300 \text{ K}$ ^{34,35} (Appendix A). We measured the conductivity for electric fields ranging from 0.025 to 0.7 V nm^{-1} . At these field amplitudes, some of the water molecules align their dipole moment along the field, but the system retains its liquid structure and the field does not disrupt the ion solvation layers (Fig. 1). The conductivity as a function of E is presented by filled circles in Fig. 2. At both concentrations, the conductivity dependence on the electric field is subtle: it slightly increases and then decreases with the electric field, with a maximum around 0.1 V nm^{-1} . To probe the effect of the alignment of the water molecules on the external field, we performed simulations where the external field was only applied to the ions¹³ (Fig. 2, open squares). In this configuration, the conductivity increases over the whole range of applied electric fields,

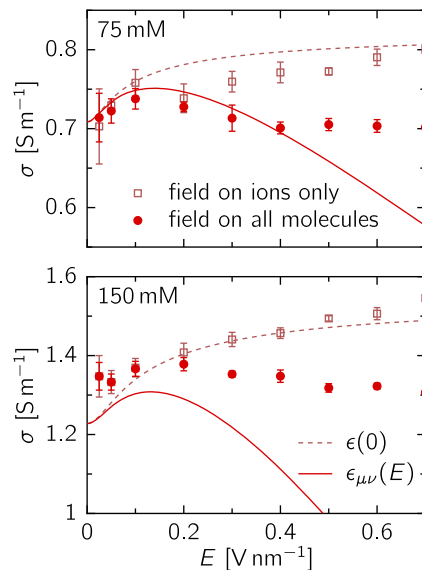


FIG. 2. Conductivity as a function of the electric field for aqueous solutions of NaCl at concentrations $\rho = 75$ and 150 mM from numerical simulations (symbols) and theory (lines). Open symbols correspond to simulations where the external electric field is only applied to the ions, while it is applied to the ions and the water molecules for closed symbols. Dashed lines are the DHO theory, with a constant water relative permittivity of $\epsilon_r = 71$; solid lines are the theory described here, which includes the effect of the electric field on the permittivity [Eqs. (4) and (5)]. The Nernst–Einstein conductivity is $\sigma_0 \approx 0.94 \text{ S m}^{-1}$ for $\rho = 75 \text{ mM}$ and $\sigma_0 \approx 1.88 \text{ S m}^{-1}$ for $\rho = 150 \text{ mM}$.

corresponding to the first Wien effect. For both concentrations, the data are quantitatively reproduced by the DHO theory without any fitting parameter (Fig. 2, dashed lines).

III. ANISOTROPIC FIELD-DEPENDENT PERMITTIVITY

From the observations above, we conclude that the nonlinear conductivity is strongly affected by the response of the water molecules to the external field. Indeed, the external field polarizes water (Fig. 1), thereby reducing the response of water molecules to extra fields such as the ones generated by the ions, that is, reducing the permittivity of the medium. Computing this effect from first principles has proven a difficult task.³⁶ Instead, we use a model where the water molecules are represented by dipoles on a lattice with magnitude p and density ρ_d ^{22,30} and allow ourselves to fit these quantities.³⁷ Note that the role of the lattice is to enforce the incompressibility of water. Neglecting the interactions between the dipoles, the free energy density under an external field with magnitude E is

$$f(E) = -\frac{\epsilon_0}{2} E^2 - \frac{\rho_d}{\beta} \log \left(\frac{\sinh(\beta p E)}{\beta p E} \right), \quad (1)$$

where ϵ_0 is the vacuum permittivity and β is the inverse thermal energy. While Ref. 30 focused on one-dimensional systems, the tensorial permittivity may be obtained as $\epsilon_{\mu\nu} = -\partial^2 f(E)/(\partial E_\mu \partial E_\nu)$.³⁸ Here, the relevant permittivity to describe the interaction between the ions is given by the expansion of this relation around the external

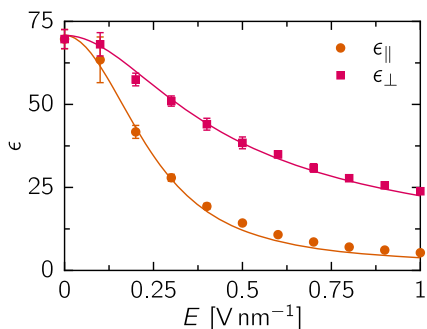


FIG. 3. Longitudinal and transverse permittivity from numerical simulations (Appendix A, symbols) and theory [solid lines, Eqs. (2) and (3)].

field, leading to a diagonal permittivity tensor with different values along the external field and transverse to it (Appendix B),

$$\epsilon_{\parallel} = \epsilon_0 + \rho_d \beta p^2 \left[\frac{1}{x^2} - \frac{1}{\sinh(x)^2} \right], \quad (2)$$

$$\epsilon_{\perp} = \epsilon_0 + \rho_d \beta p^2 \left[\frac{\coth(x)}{x} - \frac{1}{x^2} \right], \quad (3)$$

where $x = \beta p E = E/E_w$ is the dimensionless field, and $E_w = 1/(\beta p)$ being the external field necessary to orient a water molecule. Both expressions give $\epsilon_0 + \beta \rho_d p^2 / 3 = \epsilon_0 \epsilon_r$ for small fields and decay to ϵ_0 for large fields.

We simulated a solution of pure water under an increasing electrostatic field from 0 to 1 V nm⁻¹ applied along the x direction. We computed the permittivity tensor from the fluctuations of the total dipole moment \mathbf{M} of the simulation cell (Appendix A 2). The longitudinal permittivity ϵ_{\parallel} is derived from the fluctuations of M_x and the transverse permittivity ϵ_{\perp} from the fluctuations of M_y and M_z . Analytical expressions fit very well to the longitudinal and transverse permittivities measured in the simulations with $p = 3.6 \times 10^{-29}$ C m and $\rho_d = 6.0$ nm⁻³ (Fig. 3), that is, with a dipole moment that is about 5 times larger than that of the water molecule, consistent with the calculation of Booth,²² and a density that is about 5 times smaller than that of the liquid. With this value of the dipolar moment p , the field necessary to orient a water molecule is $E_w \approx 0.12$ V nm⁻¹. Beyond the decay, the permittivity tensor exhibits a strong anisotropy at intermediary fields, the transverse component being much larger than the longitudinal one.

IV. CONDUCTIVITY FROM STOCHASTIC DENSITY FIELD THEORY

The salt reduces the permittivity of water,^{39–41} but at the moderate concentrations we consider, the decrease is limited to a few percent. We, therefore, assume that the permittivity in electrolytes can be approximated to that of pure water (Fig. 3). Its anisotropy results in anisotropic electrostatic interactions between the ions; the pairwise interaction between ionic species i and j is given by $\tilde{V}_{ij}(\mathbf{k}) = q^2 z_i z_j / (\epsilon_{\parallel} k_{\parallel}^2 + \epsilon_{\perp} k_{\perp}^2)$ in Fourier space, where q is the elementary charge and z_i is the valency of the ions of type i , \mathbf{k} is the wavenumber, and k_{\parallel} and k_{\perp} are its components parallel and perpendicular to the external field, respectively. We resort to SDFT to

compute the ionic correlations. The ions are represented as point particles obeying an overdamped Langevin dynamics with mobilities κ_i under the action of the interparticle forces calculated from V_{ij} and the external field E . Using SDFT, the microscopic dynamics of the ions is mapped onto an overdamped Langevin dynamics for the density field of each species.¹⁴ Assuming small density fluctuations, which correspond to the Debye–Hückel approximation, the density dynamics can be linearized and the correlations can be computed¹⁵ (Appendix C).

The Nernst–Einstein conductivity $\sigma_0 = \rho q^2 \kappa$, where $\kappa = \kappa_+ + \kappa_-$, is reduced by the electrostatic $\Delta\sigma_{\text{el}}$ and hydrodynamic $\Delta\sigma_{\text{hyd}}$ corrections, which are deduced from the ionic correlations,^{15,18,42}

$$\frac{\Delta\sigma_{\text{el}}}{\sigma_0} = -\frac{\beta q^2 m}{4\sqrt{2\pi\epsilon_0\epsilon_r}} \int_0^1 dy \frac{y^2 \gamma_y}{\alpha_y^{3/2}}, \quad (4)$$

$$\frac{\Delta\sigma_{\text{hyd}}}{\sigma_0} = -\frac{m}{2\sqrt{2\pi\eta\kappa}} \int_0^1 dy \frac{(1-y^2)(1+\gamma_y)}{\sqrt{\alpha_y}}. \quad (5)$$

We have introduced the inverse Debye length at zero field $m = \sqrt{2\beta q^2 \rho / (\epsilon_0 \epsilon_r)}$. The anisotropic permittivity is encoded in $\alpha_y = [\epsilon_{\parallel} y^2 + \epsilon_{\perp} (1-y^2)] / (\epsilon_0 \epsilon_r)$ and $\gamma_y = \left[1 + \sqrt{2(1+F^2 y^2 \alpha_y)} \right]^{-1}$. The dimensionless electric field is defined by $F = E/E_c$, where $E_c = m/(\beta q)$ is the field necessary to destroy the ionic cloud when the permittivity is assumed to be constant. The ionic mobilities κ_i are measured via the Einstein relation in simulations of very dilute solutions without an external field (Appendix A 4). The hydrodynamic correction involves the viscosity η of the solvent, which we assume to be constant and isotropic; we use the value $\eta = 0.729 \times 10^{-3}$ Pa s.³² These expressions hold for monovalent salts; the general results are given in Appendixes D and E.

Our prediction for the conductivity, $\sigma_0 + \Delta\sigma_{\text{el}} + \Delta\sigma_{\text{hyd}}$, is shown by red solid lines in Fig. 2. For comparison, the DHO prediction, which assumes a constant isotropic permittivity $\epsilon_0 \epsilon_r$, is shown as light dashed lines. Up to electric fields of 0.4 V nm⁻¹, the agreement is quantitative for the smaller concentration, $\rho = 75$ mM; for the larger concentration, $\rho = 150$ mM, the theory underestimates the conductivity as expected,¹⁸ but the agreement is still qualitative. The conductivity predicted by DHO is an increasing function of the electric field, as measured in the simulations where the external field acts only on the ions. In contrast, our calculation predicts a nonmonotonic dependence, which is compatible with the simulations where the external field acts on all the molecules; in particular, the electric field where the conductivity is predicted to be maximal corresponds to the location of the slight maximum observed in simulations. For large electric fields, the discrepancy between theory and simulations increases: as the permittivity decays, the correlations between the ions increase, and the assumption of small density fluctuations used to compute the correlations no longer holds.

To better understand the shape of the conductivity curve, we plot the theoretical prediction for the total correction, $\Delta\sigma = \Delta\sigma_{\text{el}} + \Delta\sigma_{\text{hyd}}$, as solid lines for a wide range of concentrations and a wide range of external fields, up to unrealistic values, in Fig. 4(a). For the most dilute system, $\rho = 15$ mM, the correction first decays, which corresponds to an increase in the conductivity, and then increases;

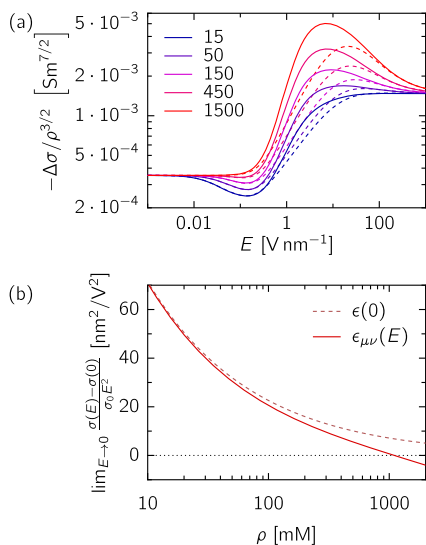


FIG. 4. (a) Rescaled correction to the Nernst-Einstein conductivity for different concentrations (indicated in mM), with the anisotropic permittivity (solid lines) and the isotropic permittivity $\epsilon = \epsilon_{\mu\mu}/3$ (dashed lines). (b) Coefficient of E^2 in the small field expansion as a function of the salt concentration.

for the densest system, $\rho = 1.5\text{M}$, the contrary is observed: the correction first increases and then decays. In the intermediate range, for instance, for $\rho = 150$ mM, the correction decreases, increases, and decreases again; the last decay is not observed in Fig. 2 as it occurs for large values of the external field, $E \gtrsim 10$ V nm⁻¹. Two nonlinear effects compete here; one is the decay of the water permittivity, which enhances the interactions and the ionic correlations, occurring at the characteristic field E_w . The other is the destruction of the ionic correlations above the characteristic field E_c . For weak electric fields, the evolution of the conductivity is the sum of the two effects (Appendices D 3 and E 3),

$$\frac{\sigma(E) - \sigma(0)}{\sigma_0} \underset{E \rightarrow 0}{\sim} a \frac{E^2}{E_c^2} + b \frac{E^2}{E_w^2}. \quad (6)$$

The coefficients a and b scale as $\sqrt{\rho}$ and have opposite signs; $a > 0$ while $b < 0$. The characteristic field E_c also scales as $\sqrt{\rho}$, while E_w is a characteristic of pure water and does not depend on the salt concentration. As a consequence, the coefficient of E^2 in Eq. (6) may change sign as a function of the salt concentration. This is shown in Fig. 4(b), where we plot this coefficient as a function of ρ for solutions associated with field-dependent permittivity (solid line) vs solutions with constant permittivity (dashed line). The change of sign occurs for concentrated solutions ($\rho \geq 1\text{M}$); however, note that the correction due to the decrease of the permittivity is barely visible for concentrations below 100 mM.

The nonmonotonic evolution of the conductivity with the external field is chiefly explained by the interplay of the destruction of the ionic correlations and the decay of the permittivity, irrespective of its anisotropy. However, considering an isotropic medium by replacing the anisotropic permittivity $\epsilon_{\mu\mu}$ with its angular averaged value $\epsilon_{\mu\mu}/3$ significantly reduces the correction $\Delta\sigma$, which is shown by the dashed lines in Fig. 4.

V. CONCLUSION

We have shown that the conductivity of aqueous electrolytes may be a nonmonotonic function of the external field, and we have explained the result by the evolution of the permittivity of water, which decreases with field strength and also becomes anisotropic. The decrease as well as the anisotropy of the permittivity can be included in SDFT to reproduce qualitatively the evolution of the conductivity and even yield quantitative predictions at low concentrations.

In the future, this integration of molecular properties of water into the analytically tractable framework of SDFT could be extended to include, for instance, a non-local permittivity $\tilde{\epsilon}(\mathbf{k})$ to account for the finite size of the water molecules^{43,44} or a frequency-dependent permittivity $\tilde{\epsilon}(\omega)$ to account for their relaxational dynamics.^{45,46} Finally, beyond the bulk conductivity of strong electrolytes, we expect that the molecular properties of water also affect ionic transport in quasi two- or one-dimensional systems, where confinement and ions control the structure of water.⁴⁷ This results in a strongly anisotropic permittivity tensor, whose eigenvalues can be significantly higher^{48,49} or lower^{47,50} than the bulk one. The inclusion of the molecular properties of the solvent in SDFT would thus allow a better description of the first and second Wien effects in such systems.^{10,11}

AUTHOR DECLARATIONS

Conflict of Interest

The authors have no conflicts to disclose.

Author Contributions

Hélène Berthoumieux: Conceptualization (equal); Data curation (equal); Formal analysis (equal); Investigation (equal); Methodology (equal); Writing – original draft (equal); Writing – review & editing (equal). **Vincent Démery:** Conceptualization (equal); Formal analysis (equal); Investigation (equal); Methodology (equal); Writing – original draft (equal); Writing – review & editing (equal). **Anthony C. Maggs:** Conceptualization (equal); Formal analysis (equal); Investigation (equal); Writing – original draft (equal); Writing – review & editing (equal).

The data that support the findings of this study are available from the corresponding author upon reasonable request. The simulation files and the codes used to interpret the simulations results are openly available on GitHub (Ref. 35).

DATA AVAILABILITY

The data that support the findings of this study are available from the corresponding author upon reasonable request. The simulation files and the codes used to interpret the simulations results are openly available on GitHub (Ref. 35).

APPENDIX A: MOLECULAR DYNAMICS SIMULATIONS

1. Simulation methods

Simulations are performed using the GROMACS 2023.2 molecular dynamics simulation package.³⁴ Simulation boxes are periodically replicated in all directions, and long-range electrostatics are handled using the smooth particle mesh Ewald (SPME) technique with tin-foil boundary conditions. Lennard-Jones interactions are

cutoff at a distance $r_{\text{cut}} = 0.9$ nm. The potential is shifted to zero at the cutoff separation. All systems are coupled to a heat bath at 300 K using a v-rescale thermostat with a time constant of 0.5 ps. We use MDAnalysis to treat the trajectories.

After creating the system, we first perform energy minimization. We then equilibrate the system in the NVT ensemble for 200 ps, and then in the NPT ensemble for another 200 ps using a Berendsen barostat at 1 bar. Production runs are performed in the NVT ensemble. The integration time step is set to $\Delta t = 2$ fs.

2. Permittivity of pure water under electrostatic field

We simulate a cubic box of pure water of side size $L = 6.5$ nm. We use the SPC/E model for water,^{31,32} a three-point charge and one Lennard-Jones reference site model. The Lennard-Jones (LJ) center is placed on the oxygen. Charges are placed on the hydrogen atoms and the oxygen.

During the production run, we apply a static electrostatic field along the x -axis to the system using the option “electric-field-x: $E \ 0 \ 0 \ 0$.” We perform 11 production runs of 20 ns, varying the amplitude of E from 0 to 1 V nm⁻¹ with a step of 0.1 V nm⁻¹.

In an external field, the permittivity of water is an anisotropic, diagonal tensor characterized by a component ϵ_{\parallel} , aligned with the field direction x , and a perpendicular component ϵ_{\perp} in the (y, z) plane. We calculate this tensor from the total system dipole moment⁵¹ \mathbf{M} that we compute for each frame after dropping the first nanosecond of the run. It is defined as the volume integral of the polarization \mathcal{P} and $\mathbf{M} = \int_V \mathcal{P}(\mathbf{r}) d\mathbf{r}$, where V is the volume of the box. The permittivity obeys

$$\epsilon_{\parallel} = \frac{\langle M_x^2 \rangle - \langle M_x \rangle^2}{\epsilon_0 k_B TV} + 1, \quad (\text{A1})$$

$$\epsilon_{\perp} = \frac{\langle M_y^2 \rangle + \langle M_z^2 \rangle - \langle M_y \rangle^2 - \langle M_z \rangle^2}{2\epsilon_0 k_B TV} + 1. \quad (\text{A2})$$

3. Field-dependent conductivity of aqueous electrolyte solution

We simulate a cubic aqueous electrolyte box of size $L = 6.5$ nm. The 150 mM solution contains 8875 water molecules and 25 ion pairs of (Na^+ , Cl^-); the 75 mM solution contains 8901 water molecules and 12 ion pairs. The Debye length of the electrolyte is equal to 0.7 nm, respectively, 1.1 nm, which is significantly smaller than the box size. We take the following LJ parameters ($\sigma_{\text{Na}} = 0.231$ nm, $\epsilon_{\text{Na}} = 0.45$ kJ mol⁻¹) and ($\sigma_{\text{Cl}} = 0.43$ nm, $\epsilon_{\text{Cl}} = 0.42$ kJ mol⁻¹),³³ and we use the Lorentz–Berthelot mixing rules for the LJ interactions.

For the first set of simulations, we proceed as for pure water and apply a static electrostatic field along the x -axis during the production run. We perform nine runs for which we vary the amplitude of E from 0.025 to 0.7 V nm⁻¹.

For the second set of simulations, only the ions (Na^+ , Cl^-) feel the electrostatic field and not the water charges. We impose an acceleration $a_{\text{Na}} = qE/m_{\text{Na}}$ to the cations and $a_{\text{Cl}} = -qE/m_{\text{Cl}}$ to the anions along the x axis, where q is the elementary charge and m_i is the molar mass of the species i . It corresponds to the acceleration induced by

an electrostatic field of amplitude E . We take $m_{\text{Na}} = 22.990$ g mol⁻¹ and $m_{\text{Cl}} = 35.450$ g mol⁻¹.

For the two sets of simulations, we perform runs of 200 ns for the two lowest fields ($E = 0.025$ V nm⁻¹ and $E = 0.05$ V nm⁻¹) and of 20 ns for the higher fields.

For each run, we measure the average velocity of the anions v_{cl} and cations v_{Na} after dropping the first nanosecond of the run, and we compute the conductivity with

$$\sigma(E) = \frac{q\rho(v_{\text{Na}} - v_{\text{Cl}})}{E}, \quad (\text{A3})$$

with ρ being the ionic density.

4. Estimation of the ion mobility

We use a very dilute regime to compute the mobility of the ions. We simulate a cubic box of aqueous electrolyte of side $L = 10$ nm. The 10 mM solution contains six pairs of (Na^+ , Cl^-) and 32 761 water molecules. After equilibration following the procedure described in Appendix A 1, we perform a simulation run of 40 ns and evaluate the diffusion coefficient of the ions from the mean square displacement using the command “gmx msd.” We obtain $D_{\text{Na}} = 1.2813(3351) \times 10^{-9}$ m²/s and $D_{\text{Cl}} = 2.0514(2811) \times 10^{-9}$ m²/s. We calculate mobilities using the Einstein relation $\kappa_i = D_i/k_B T$,

$$\kappa_{\text{Na}} = 3.0935(8090) \times 10^{11} \text{ m s}^{-1} \text{ N}^{-1}, \quad (\text{A4})$$

$$\kappa_{\text{Cl}} = 4.9527(6787) \times 10^{11} \text{ m s}^{-1} \text{ N}^{-1}. \quad (\text{A5})$$

5. Statistical treatment

For the parallel and perpendicular permittivity [Eqs. (A1) and (A2)] and for the conductivity [Eq. (A3)], we compute the error bars with the reblocking method.⁵²

APPENDIX B: ANISOTROPIC PERMITTIVITY FOR DIPOLES ON A LATTICE

Here, we derive the anisotropic permittivity [Eqs. (2) and (3)] from the free energy density (1) for dipoles on a lattice.

The permittivity tensor is given by $\epsilon_{\mu\nu} = -\partial^2 f(E)/(\partial E_\mu \partial E_\nu)$. Using the fact that the free energy density $f(E)$ depends only on the magnitude of the electric field and denoting its derivatives with primes, we find

$$\epsilon_{\mu\nu} = -\delta_{\mu\nu} \frac{f'(E)}{E} + \frac{E_\mu E_\nu}{E^2} \left[\frac{f'(E)}{E} - f''(E) \right]. \quad (\text{B1})$$

Along the field $E_\mu E_\nu = E^2$, while transverse to it $E_\mu E_\nu = 0$, which leads to

$$\epsilon_{\parallel} = -f''(E), \quad (\text{B2})$$

$$\epsilon_{\perp} = -\frac{f'(E)}{E}. \quad (\text{B3})$$

The derivatives of the free energy density are given by

$$f'(E) = -\varepsilon_0 E - \rho_d p \left[\coth(x) - \frac{1}{x} \right], \quad (\text{B4})$$

$$f''(E) = -\varepsilon_0 - \beta \rho_d p^2 \left[\frac{1}{x^2} - \frac{1}{\sinh(x)^2} \right]. \quad (\text{B5})$$

Inserting these derivatives in Eqs. (B2) and (B3) leads to the expressions (2, 3).

APPENDIX C: CORRELATIONS FROM SDFT

Ionic correlations have been computed for arbitrary interactions in Ref. 15. The operators $\tilde{R}(\mathbf{k})$ and $\tilde{A}(\mathbf{k})$ of Eqs. (15) and (16) in Ref. 15 are given by

$$\tilde{R}(\mathbf{k}) = k^2 \begin{pmatrix} \bar{\rho}_+ \kappa_+ & 0 \\ 0 & \bar{\rho}_- \kappa_- \end{pmatrix} = k^2 \begin{pmatrix} r_+ & 0 \\ 0 & r_- \end{pmatrix}, \quad (\text{C1})$$

$$\tilde{A}(\mathbf{k}) = \beta^{-1} \begin{pmatrix} \frac{1}{\bar{\rho}_+} \left(1 + i \frac{\beta z_+ q E \cdot \mathbf{k}}{k^2} \right) + \beta \tilde{V}_{++}(\mathbf{k}) & \beta \tilde{V}_{+-}(\mathbf{k}) \\ \beta \tilde{V}_{+-}(\mathbf{k}) & \frac{1}{\bar{\rho}_-} \left(1 + i \frac{\beta z_- q E \cdot \mathbf{k}}{k^2} \right) + \beta \tilde{V}_{--}(\mathbf{k}) \end{pmatrix} = \beta^{-1} \begin{pmatrix} a & b \\ b & c \end{pmatrix}, \quad (\text{C2})$$

with $\bar{\rho}_i$ being the mean density of ions of type i . We still use electrostatic interactions,

$$\tilde{V}_{\alpha\beta}(\mathbf{k}) = q^2 z_\alpha z_\beta \tilde{G}_0(\mathbf{k}), \quad (\text{C3})$$

where here, with $\varepsilon = \varepsilon_0 \varepsilon_r$,

$$\tilde{G}_0(\mathbf{k}) = \frac{1}{\varepsilon(\alpha_{\parallel} k_{\parallel}^2 + \alpha_{\perp} k_{\perp}^2)} = \frac{\tilde{g}(\mathbf{k})}{\varepsilon}. \quad (\text{C4})$$

The general form of the correlation $\tilde{C}(\mathbf{k})$ is given in Eq. (24) of Ref. 15,

$$\begin{aligned} \tilde{C} = & \frac{2}{(a + a^*)(c + c^*)|r_+ a + r_- c^*|^2 - b^2[r_+(a + a^*) + r_-(c + c^*)]^2} \\ & \times \begin{pmatrix} (c + c^*)|r_+ a + r_- c^*|^2 & -b(r_+ a^* + r_- c)[r_+(a + a^*) + r_-(c + c^*)] \\ -b(r_+ a + r_- c^*)[r_+(a + a^*) + r_-(c + c^*)] & (a + a^*)|r_+ a + r_- c^*|^2 \end{pmatrix}. \end{aligned} \quad (\text{C5})$$

With the notations,

$$\kappa = \kappa_+ + \kappa_-, \quad (\text{C6})$$

$$m^2 = m_+^2 + m_-^2, \quad (\text{C9})$$

$$\kappa' = \kappa_+ z_+ - \kappa_- z_-, \quad (\text{C7})$$

$$m'^2 = \frac{\kappa_+ m_+^2 + \kappa_- m_-^2}{\kappa_+ + \kappa_-} = \frac{\beta \sigma_0}{\varepsilon(\kappa_+ + \kappa_-)}, \quad (\text{C10})$$

$$m_\alpha^2 = \frac{\beta q^2 z_\alpha^2 \bar{\rho}_\alpha}{\varepsilon}, \quad (\text{C8})$$

$$F = \frac{\beta q E}{m} = \frac{E}{E_c}, \quad (\text{C11})$$

the correlation reads

$$\begin{aligned} \tilde{C} = & \left[\kappa^2 (1 + m^2 \tilde{g})(1 + m'^2 \tilde{g})^2 + \kappa'^2 m^2 (1 + m_+^2 \tilde{g})(1 + m_-^2 \tilde{g}) \left(\frac{F k_{\parallel}}{k^2} \right)^2 \right]^{-1} \\ & \times \begin{pmatrix} \bar{\rho}_+ (1 + m_-^2 \tilde{g}) \left[\kappa^2 (1 + m'^2 \tilde{g})^2 + \kappa'^2 m^2 \left(\frac{F k_{\parallel}}{k^2} \right)^2 \right] & \sqrt{\bar{\rho}_+ \bar{\rho}_-} \kappa m_+ m_- \tilde{g} (1 + m'^2 \tilde{g}) \left[\kappa (1 + m'^2 \tilde{g}) - i \kappa' m \frac{F k_{\parallel}}{k^2} \right] \\ \sqrt{\bar{\rho}_+ \bar{\rho}_-} \kappa m_+ m_- \tilde{g} (1 + m'^2 \tilde{g}) \left[\kappa (1 + m'^2 \tilde{g}) + i \kappa' m \frac{F k_{\parallel}}{k^2} \right] & \bar{\rho}_- (1 + m_+^2 \tilde{g}) \left[\kappa^2 (1 + m'^2 \tilde{g})^2 + \kappa'^2 m^2 \left(\frac{F k_{\parallel}}{k^2} \right)^2 \right] \end{pmatrix}. \end{aligned} \quad (\text{C12})$$

APPENDIX D: ELECTROSTATIC CORRECTION TO THE CONDUCTIVITY

1. General case

Using Eq. (25) in Ref. 15, we find the electrostatic correction to the conductivity in a d -dimensional space,

$$\frac{\Delta\sigma}{\sigma_0} = \frac{q^3}{\sigma_0 \epsilon E} \sum_{\alpha, \beta} \kappa_\alpha z_\alpha z_\beta \int ik_\parallel \tilde{g} \tilde{C}_{\alpha\beta}(\mathbf{k}) \frac{d\mathbf{k}}{(2\pi)^d}, \quad (\text{D1})$$

$$= -\frac{\beta q^2 \kappa'^2 m_+^2 m_-^2}{\epsilon m'^2} \int \frac{k_\parallel^2 \tilde{g}^2 (1 + m'^2 \tilde{g})}{k^2 \left[\kappa^2 (1 + m^2 \tilde{g}) (1 + m'^2 \tilde{g})^2 + \kappa'^2 m^2 (1 + m_+^2 \tilde{g}) (1 + m_-^2 \tilde{g}) \left(\frac{F k_\parallel}{k^2} \right)^2 \right]} \frac{d\mathbf{k}}{(2\pi)^d}. \quad (\text{D2})$$

To integrate the correction numerically, we specify the calculation to $d = 3$, and we change the integration variable from \mathbf{k} to $u \in [0, \infty)$ and $y \in [-1, 1]$ with $\mathbf{k} = mu$ and $y = u_\parallel/u$ and $d\mathbf{k} = 2\pi m^3 u^2 dy du$. The Green function reads $\tilde{g} = (m^2 u^2 \alpha_y)^{-1}$ [Eq. (C4)] with $\alpha_y = [\epsilon y^2 + \epsilon_\perp (1 - y^2)]/\epsilon$, and the correction is given by

$$\frac{\Delta\sigma}{\sigma_0} = -\frac{\beta q^2 m_+^2 m_-^2 m^3}{(2\pi)^2 \epsilon m'^2} \int_0^\infty du \int_{-1}^1 dy \frac{y^2 u^2 \tilde{g}^2 (1 + m'^2 \tilde{g})}{\kappa^2 (1 + m^2 \tilde{g}) (1 + m'^2 \tilde{g})^2 + (1 + m_+^2 \tilde{g}) (1 + m_-^2 \tilde{g}) \frac{F^2 y^2}{u^2}}, \quad (\text{D3})$$

$$= -\frac{\beta q^2 m \mu_+^2 \mu_-^2}{(2\pi)^2 \epsilon \mu'^2} \int_0^\infty du \int_{-1}^1 dy \frac{y^2 \left(1 + \frac{\mu'^2}{u^2 \alpha_y} \right)}{\alpha_y^2 u^2 \left[\frac{\kappa^2}{\kappa'^2} \left(1 + \frac{1}{u^2 \alpha_y} \right) \left(1 + \frac{\mu'^2}{u^2 \alpha_y} \right)^2 + \left(1 + \frac{\mu_+^2}{u^2 \alpha_y} \right) \left(1 + \frac{\mu_-^2}{u^2 \alpha_y} \right) \frac{F^2 y^2}{u^2} \right]}, \quad (\text{D4})$$

$$= -\frac{\beta q^2 m \mu_+^2 \mu_-^2}{2\pi^2 \epsilon \mu'^2} \int_0^\infty du \int_0^1 dy \frac{y^2 u^2 (\alpha_y u^2 + \mu'^2)}{\frac{\kappa^2}{\kappa'^2} (\alpha_y u^2 + 1) (\alpha_y u^2 + \mu'^2)^2 + F^2 y^2 \alpha_y (\alpha_y u^2 + \mu_+^2) (\alpha_y u^2 + \mu_-^2)}. \quad (\text{D5})$$

We have introduced $\mu' = m'/m$, $\mu_\pm = m_\pm/m$, and used the fact that the integral is even in y .

2. Monovalent salt

For a monovalent salt, $z_+ = -z_- = 1$ and $\rho_+ = \rho_-$, so that $m_i^2 = m'^2 = m^2/2$, $\kappa' = \kappa$, and $\mu_i = \mu' = 1/\sqrt{2}$. The expression above simplifies to

$$\frac{\Delta\sigma_{\text{el}}}{\sigma_0} = -\frac{\beta q^2 m}{2\pi^2 \epsilon} \int_0^\infty du \int_0^1 dy \frac{y^2 u^2}{(2u^2 \alpha_y + 1)(u^2 \alpha_y + 1 + F^2 y^2 \alpha_y)} = -\frac{\beta q^2 m}{4\sqrt{2}\pi \epsilon_0 \epsilon_r} \int_0^1 \frac{y^2 dy}{\alpha_y^{3/2} \left[1 + \sqrt{2(1 + F^2 y^2 \alpha_y)} \right]}. \quad (\text{D6})$$

3. Small field expansion

We write the electrostatic correction as

$$\frac{\Delta\sigma_{\text{el}}}{\sigma_0} = -\frac{\beta q^2 m \mu_+^2 \mu_-^2}{2\pi^2 \epsilon \mu'^2} s_e, \quad (\text{D7})$$

with

$$s_e = \int_0^\infty du \int_0^1 dy \frac{y^2 u^2 (\alpha_y u^2 + \mu'^2)}{\frac{\kappa^2}{\kappa'^2} (\alpha_y u^2 + 1) (\alpha_y u^2 + \mu'^2)^2 + F^2 y^2 \alpha_y (\alpha_y u^2 + \mu_+^2) (\alpha_y u^2 + \mu_-^2)}. \quad (\text{D8})$$

After a few lines of calculation, we get at order E^2 ,

$$s_e = \frac{\kappa'^2}{3\kappa^2} \int_0^\infty du \frac{u^2}{(1 + u^2)(u^2 + \mu'^2)} - \frac{\kappa'^4}{5\kappa^4} F^2 \int_0^\infty du \frac{u^2 (u^2 + \mu_+^2)(u^2 + \mu_-^2)}{(u^2 + 1)^2 (u^2 + \mu'^2)^3} + \frac{11}{225} \frac{\kappa'^2}{\kappa^2} \frac{\epsilon_r - 1}{\epsilon_r} x^2 \int_0^\infty du \frac{u^4 (2u^2 + 1 + \mu'^2)}{(u^2 + 1)^2 (u^2 + \mu'^2)^2}, \quad (\text{D9})$$

where $F = E/E_c$ and $x = E/E_w$.

APPENDIX E: HYDRODYNAMIC CORRECTION TO THE CONDUCTIVITY

1. General case

The hydrodynamic correction to the conductivity is [Eq. (17) in Ref. 42]

$$\frac{\Delta\sigma_{\text{hyd}}}{\sigma_0} = q^2 \int \tilde{\mathcal{O}}_{11}(\mathbf{k}) \sum_{\alpha\beta} z_\alpha z_\beta [\tilde{C}_{\alpha\beta}(\mathbf{k}) - \bar{\rho}_\alpha \delta_{\alpha\beta}] \frac{d\mathbf{k}}{(2\pi)^d}. \quad (\text{E1})$$

Using the correlation (C12), we find

$$\frac{\Delta\sigma_{\text{hyd}}}{\sigma_0} = -\frac{q^2}{\eta\sigma_0} \int \frac{d\mathbf{k}}{(2\pi)^d} \frac{k_\perp^2}{k^4} \tilde{g} \frac{\kappa^2 (1 + m'^2 \tilde{g})^2 (z_+ \sqrt{\bar{\rho}_+} m_+ + z_- \sqrt{\bar{\rho}_-} m_-)^2 + \kappa'^2 m^2 [z_+^2 \bar{\rho}_+ m_+^2 (1 + m_-^2 \tilde{g}) + z_-^2 \bar{\rho}_- m_-^2 (1 + m_+^2 \tilde{g})] \left(\frac{F k_\parallel}{k^2}\right)^2}{\kappa^2 (1 + m^2 \tilde{g}) (1 + m'^2 \tilde{g})^2 + \kappa'^2 m^2 (1 + m_+^2 \tilde{g}) (1 + m_-^2 \tilde{g}) \left(\frac{F k_\parallel}{k^2}\right)^2}. \quad (\text{E2})$$

To perform the numerical integration, we follow the same steps as for the electrostatic correction,

$$\frac{\Delta\sigma_{\text{hyd}}}{\sigma_0} = -\frac{q^2 m}{(2\pi)^2 \eta\sigma_0} \int_0^\infty du \int_{-1}^1 dy (1 - y^2) \tilde{g} \frac{\frac{\kappa^2}{\kappa'^2} (1 + m'^2 \tilde{g})^2 (\sum_\alpha z_\alpha \sqrt{\bar{\rho}_\alpha} m_\alpha)^2 + [z_+^2 \bar{\rho}_+ m_+^2 (1 + m_-^2 \tilde{g}) + z_-^2 \bar{\rho}_- m_-^2 (1 + m_+^2 \tilde{g})] \frac{F^2 y^2}{u^2}}{\frac{\kappa^2}{\kappa'^2} (1 + m^2 \tilde{g}) (1 + m'^2 \tilde{g})^2 + (1 + m_+^2 \tilde{g}) (1 + m_-^2 \tilde{g}) \frac{F^2 y^2}{u^2}}, \quad (\text{E3})$$

$$= -\frac{q^2 m}{(2\pi)^2 \eta\sigma_0} \int_0^\infty du \int_{-1}^1 dy \frac{1 - y^2}{u^2 \alpha_y} \frac{\frac{\kappa^2}{\kappa'^2} \left(1 + \frac{\mu'^2}{u^2 \alpha_y}\right)^2 (\sum_\alpha z_\alpha \sqrt{\bar{\rho}_\alpha} \mu_\alpha)^2 + \left[z_+^2 \bar{\rho}_+ \mu_+^2 \left(1 + \frac{\mu_-^2}{u^2 \alpha_y}\right) + z_-^2 \bar{\rho}_- \mu_-^2 \left(1 + \frac{\mu_+^2}{u^2 \alpha_y}\right)\right] \frac{F^2 y^2}{u^2}}{\frac{\kappa^2}{\kappa'^2} \left(1 + \frac{1}{u^2 \alpha_y}\right) \left(1 + \frac{\mu'^2}{u^2 \alpha_y}\right)^2 + \left(1 + \frac{\mu_+^2}{u^2 \alpha_y}\right) \left(1 + \frac{\mu_-^2}{u^2 \alpha_y}\right) \frac{F^2 y^2}{u^2}}, \quad (\text{E4})$$

$$= -\frac{q^2 m}{2\pi^2 \eta\sigma_0} \int_0^\infty du \int_0^1 dy (1 - y^2) \frac{\frac{\kappa^2}{\kappa'^2} (u^2 \alpha_y + \mu'^2)^2 (\sum_\alpha z_\alpha \sqrt{\bar{\rho}_\alpha} \mu_\alpha)^2 + F^2 y^2 \alpha_y [z_+^2 \bar{\rho}_+ \mu_+^2 (u^2 \alpha_y + \mu_-^2) + z_-^2 \bar{\rho}_- \mu_-^2 (u^2 \alpha_y + \mu_+^2)]}{\frac{\kappa^2}{\kappa'^2} (u^2 \alpha_y + 1) (u^2 \alpha_y + \mu'^2)^2 + F^2 y^2 \alpha_y (u^2 \alpha_y + \mu_+^2) (u^2 \alpha_y + \mu_-^2)}. \quad (\text{E5})$$

2. Monovalent salt

For a monovalent salt, the expression above simplifies into

$$\begin{aligned} \frac{\Delta\sigma_{\text{hyd}}}{\sigma_0} &= -\frac{m}{\pi^2 \eta \kappa} \int_0^\infty du \int_0^1 dy \frac{(1 - y^2)(2u^2 \alpha_y + 1 + F^2 y^2 \alpha_y)}{(2u^2 \alpha_y + 1)(u^2 \alpha_y + 1 + F^2 y^2 \alpha_y)} \\ &= -\frac{m}{2\sqrt{2\pi} \eta \kappa} \int_0^1 dy \frac{1 - y^2}{\sqrt{\alpha_y}} \left[1 + \frac{1}{1 + \sqrt{2(1 + F^2 y^2 \alpha_y)}} \right]. \end{aligned} \quad (\text{E6})$$

3. Small field expansion

For the hydrodynamic correction, we denote

$$\frac{\Delta\sigma_{\text{hyd}}}{\sigma_0} = -\frac{q^2 m}{2\pi^2 \eta \sigma_0} s_h, \quad (\text{E7})$$

where

$$s_h = \int_0^\infty du \int_0^1 dy (1 - y^2) \frac{\frac{\kappa^2}{\kappa'^2} (u^2 \alpha_y + \mu'^2)^2 (\sum_i z_i \sqrt{\bar{\rho}_i} \mu_i)^2 + F^2 y^2 \alpha_y [z_+^2 \bar{\rho}_+ \mu_+^2 (u^2 \alpha_y + \mu_-^2) + z_-^2 \bar{\rho}_- \mu_-^2 (u^2 \alpha_y + \mu_+^2)]}{\frac{\kappa^2}{\kappa'^2} (u^2 \alpha_y + 1) (u^2 \alpha_y + \mu'^2)^2 + F^2 y^2 \alpha_y (u^2 \alpha_y + \mu_+^2) (u^2 \alpha_y + \mu_-^2)}. \quad (\text{E8})$$

Using the same approach, we find at order E^2 ,

$$\begin{aligned} s_h &= \frac{\pi}{3} \left(\sum_i \sqrt{z_i^2 \mu_i^2 \bar{\rho}_i} \right)^2 + \frac{7\pi}{450} \frac{\varepsilon_r - 1}{\varepsilon_r} \left(\sum_i \sqrt{z_i^2 \mu_i^2 \bar{\rho}_i} \right)^2 x^2 + \frac{2}{15} \frac{\kappa'^2}{\kappa^2} F^2 \left[\int_0^\infty du \frac{z_+^2 \bar{\rho}_+ \mu_+^2 (u^2 + \mu_-^2) + z_-^2 \bar{\rho}_- \mu_-^2 (u^2 + \mu_+^2)}{(u^2 + 1)(u^2 + \mu'^2)^2} \right. \\ &\quad \left. - \left(\sum_i \sqrt{z_i^2 \mu_i^2 \bar{\rho}_i} \right)^2 \int_0^\infty du \frac{(u^2 + \mu_+^2)(u^2 + \mu_-^2)}{(u^2 + 1)^2 (u^2 + \mu'^2)^2} \right], \end{aligned} \quad (\text{E9})$$

where $F = E/E_c$ and $x = E/E_w$.

REFERENCES

- ¹H. C. Eckstrom and C. Schmelzer, "The wien effect: Deviations of electrolytic solutions from ohm's law under high field strengths," *Chem. Rev.* **24**, 367–414 (1939).
- ²W. S. Wilson, "The theory of the Wien effect for a binary electrolyte," Ph.D. thesis (Yale University, 1936).
- ³P. Debye and E. Hückel, "Theory of electrolytes—Part II: Law of the limit of electrolytic conduction," *Phys. Z.* **24**, 305–325 (1923).
- ⁴L. Onsager, "Report on a revision of the conductivity theory," *Trans. Faraday Soc.* **23**, 341–349 (1927).
- ⁵L. Onsager and S. K. Kim, "Wien effect in simple strong electrolytes," *J. Phys. Chem.* **61**, 198–215 (1957).
- ⁶L. Onsager, "Deviations from Ohm's law in weak electrolytes," *J. Chem. Phys.* **2**, 599–615 (1934).
- ⁷J. Feng, K. Liu, M. Graf, D. Dumcenco, A. Kis, M. Di Ventra, and A. Radenovic, "Observation of ionic Coulomb blockade in nanopores," *Nat. Mater.* **15**, 850–855 (2016).
- ⁸J. Cai, E. Griffin, V. H. Guarachico-Moreira, D. Barry, B. Xin, M. Yagmurcukardes, S. Zhang, A. K. Geim, F. M. Peeters, and M. Lozada-Hidalgo, "Wien effect in interfacial water dissociation through proton-permeable graphene electrodes," *Nat. Commun.* **13**, 5776 (2022).
- ⁹A. Montenegro, C. Dutta, M. Mammetkuliev, H. Shi, B. Hou, D. Bhattacharyya, B. Zhao, S. B. Cronin, and A. V. Benderskii, "Asymmetric response of interfacial water to applied electric fields," *Nature* **594**, 62–65 (2021).
- ¹⁰P. Robin, T. Emmerich, A. Ismail, A. Niguès, Y. You, G.-H. Nam, A. Keerthi, A. Siria, A. K. Geim, B. Radha, and L. Bocquet, "Long-term memory and synapse-like dynamics in two-dimensional nanofluidic channels," *Science* **379**, 161–167 (2023).
- ¹¹P. Robin, N. Kavokine, and L. Bocquet, "Modeling of emergent memory and voltage spiking in ionic transport through angstrom-scale slits," *Science* **373**, 687–691 (2021).
- ¹²D. Lesnicki, C. Y. Gao, B. Rotenberg, and D. T. Limmer, "Field-dependent ionic conductivities from generalized fluctuation-dissipation relations," *Phys. Rev. Lett.* **124**, 206001 (2020).
- ¹³D. Lesnicki, C. Y. Gao, D. T. Limmer, and B. Rotenberg, "On the molecular correlations that result in field-dependent conductivities in electrolyte solutions," *J. Chem. Phys.* **155**, 014507 (2021).
- ¹⁴D. S. Dean, "Langevin equation for the density of a system of interacting Langevin processes," *J. Phys. A: Math. Gen.* **29**, L613–L617 (1996).
- ¹⁵V. Démery and D. S. Dean, "The conductivity of strong electrolytes from stochastic density functional theory," *J. Stat. Mech.: Theory Exp.* **2016**, 023106.
- ¹⁶J.-P. Péraud, A. J. Nonaka, J. B. Bell, A. Donev, and A. L. Garcia, "Fluctuation-enhanced electric conductivity in electrolyte solutions," *Proc. Natl. Acad. Sci. U. S. A.* **114**, 10829–10833 (2017).
- ¹⁷A. Donev, A. L. Garcia, J.-P. Péraud, A. J. Nonaka, and J. B. Bell, "Fluctuating hydrodynamics and Debye-Hückel-Onsager theory for electrolytes," *Curr. Opin. Electrochem.* **13**, 1–10 (2019).
- ¹⁸Y. Avni, R. M. Adar, D. Andelman, and H. Orland, "Conductivity of concentrated electrolytes," *Phys. Rev. Lett.* **128**, 098002 (2022).
- ¹⁹Y. Avni, D. Andelman, and H. Orland, "Conductance of concentrated electrolytes: Multivalency and the Wien effect," *J. Chem. Phys.* **157**, 154502 (2022).
- ²⁰O. Bernard, M. Jardat, B. Rotenberg, and P. Illien, "On analytical theories for conductivity and self-diffusion in concentrated electrolytes," *J. Chem. Phys.* **159**, 164105 (2023).
- ²¹J.-F. Dufrêche, O. Bernard, S. Durand-Vidal, and P. Turq, "Analytical theories of transport in concentrated electrolyte solutions from the MSA," *J. Phys. Chem. B* **109**, 9873–9884 (2005).
- ²²F. Booth, "The dielectric constant of water and the saturation effect," *J. Chem. Phys.* **19**, 391–394 (1951).
- ²³A. Piekarz and S. Kielich, "Theory of orientational effects and related phenomena in dielectric liquids," *J. Chem. Phys.* **29**, 1297–1305 (1958).
- ²⁴I.-C. Yeh and M. L. Berkowitz, "Dielectric constant of water at high electric fields: Molecular dynamics study," *J. Chem. Phys.* **110**, 7935–7942 (1999).
- ²⁵H. A. Kotodziej, G. P. Jones, and M. Davies, "High field dielectric measurements in water," *J. Chem. Soc., Faraday Trans. 2* **71**, 269–274 (1975).
- ²⁶E. N. D. C. Andrade and C. Dodd, "The effect of an electric field on the viscosity of liquids," *Proc. R. Soc. London, Ser. A* **187**, 296–337 (1946).
- ²⁷J. Lyklema and J. Overbeek, "On the interpretation of electrokinetic potentials," *J. Colloid Sci.* **16**, 501–512 (1961).
- ²⁸D. Zong, H. Hu, Y. Duan, and Y. Sun, "Viscosity of water under electric field: Anisotropy induced by redistribution of hydrogen bonds," *J. Phys. Chem. B* **120**, 4818–4827 (2016).
- ²⁹D. Jin, Y. Hwang, L. Chai, N. Kampf, and J. Klein, "Direct measurement of the viscoelectric effect in water," *Proc. Natl. Acad. Sci. U. S. A.* **119**, e2113690119 (2022).
- ³⁰A. Abrashkin, D. Andelman, and H. Orland, "Dipolar Poisson-Boltzmann equation: Ions and dipoles close to charge interfaces," *Phys. Rev. Lett.* **99**, 077801 (2007).
- ³¹H. J. C. Berendsen, J. R. Grigera, and T. P. Straatsma, "The missing term in effective pair potentials," *J. Phys. Chem.* **91**, 6269–6271 (1987).
- ³²P. E. Smith and W. F. van Gunsteren, "The viscosity of SPC and SPC/E water at 277 and 300 K," *Chem. Phys. Lett.* **215**, 315–318 (1993).
- ³³P. Loche, P. Steinbrunner, S. Friedowitz, R. R. Netz, and D. J. Bonhuis, "Transferable ion force fields in water from a simultaneous optimization of ion solvation and ion-ion interaction," *J. Phys. Chem. B* **125**, 8581–8587 (2021).
- ³⁴B. Hess, C. Kutzner, D. van der Spoel, and E. Lindahl, "Gromacs 4: Algorithms for highly efficient, load-balanced, and scalable molecular simulation," *J. Chem. Theory Comput.* **4**, 435–447 (2008).
- ³⁵See this GitHub repository for the simulation files and the Python codes used to interpret the simulations results.
- ³⁶R. L. Fulton, "The nonlinear dielectric behavior of water: Comparisons of various approaches to the nonlinear dielectric increment," *J. Chem. Phys.* **130**, 204503 (2009).
- ³⁷H. Berthoumieux, G. Monet, and R. Blossey, "Dipolar Poisson models in a dual view," *J. Chem. Phys.* **155**, 024112 (2021).
- ³⁸L. D. Landau, J. S. Bell, M. Kearsley, L. Pitaevskii, E. Lifshitz, and J. Sykes, *Electrodynamics of Continuous Media* (Elsevier, 2013), Vol. 8.
- ³⁹J. B. Hasted, D. M. Ritson, and C. H. Collie, "Dielectric properties of aqueous ionic solutions. Parts I and II," *J. Chem. Phys.* **16**, 1–21 (1948).
- ⁴⁰A. Levy, D. Andelman, and H. Orland, "Dielectric constant of ionic solutions: A field-theory approach," *Phys. Rev. Lett.* **108**, 227801 (2012).
- ⁴¹S. Seal, K. Doblhoff-Dier, and J. Meyer, "Dielectric decrement for aqueous NaCl solutions: Effect of ionic charge scaling in nonpolarizable water force fields," *J. Phys. Chem. B* **123**, 9912–9921 (2019).
- ⁴²H. Bonneau, V. Démery, and E. Raphaël, "Temporal response of the conductivity of electrolytes," *J. Stat. Mech.: Theory Exp.* **2023**, 073205.
- ⁴³P. A. Bopp, A. A. Kornyshev, and G. Sutmann, "Static nonlocal dielectric function of liquid water," *Phys. Rev. Lett.* **76**, 1280–1283 (1996).
- ⁴⁴H. Berthoumieux, "Gaussian field model for polar fluids as a function of density and polarization: Toward a model for water," *J. Chem. Phys.* **148**, 104504 (2018).
- ⁴⁵P. A. Bopp, A. A. Kornyshev, and G. Sutmann, "Frequency and wave-vector dependent dielectric function of water: Collective modes and relaxation spectra," *J. Chem. Phys.* **109**, 1939–1958 (1998).
- ⁴⁶P. Illien, A. Carof, and B. Rotenberg, "Stochastic density functional theory for ions in a polar solvent," arXiv:2407.17232 [cond-mat.soft] (2024).
- ⁴⁷H. Jalali, E. Lotfi, R. Boya, and M. Neek-Amal, "Abnormal dielectric constant of nanoconfined water between graphene layers in the presence of salt," *J. Phys. Chem. B* **125**, 1604–1610 (2021).
- ⁴⁸P. Loche, C. Ayaz, A. Schlaich, Y. Uematsu, and R. R. Netz, "Giant axial dielectric response in water-filled nanotubes and effective electrostatic ion-ion interactions from a tensorial dielectric model," *J. Phys. Chem. B* **123**, 10850–10857 (2019).

⁴⁹R. Wang, M. Souilamas, A. Esfandiar, R. Fabregas, S. Benaglia, H. Nevison-Andrews, Q. Yang, J. Normansell, P. Ares, G. Ferrari, A. Principi, A. K. Geim, and L. Fumagalli, “In-plane dielectric constant and conductivity of confined water,” [arXiv:2407.21538](https://arxiv.org/abs/2407.21538) [cond-mat.mes-hall] (2024).

⁵⁰L. Fumagalli, A. Esfandiar, R. Fabregas, S. Hu, P. Ares, A. Janardanan, Q. Yang, B. Radha, T. Taniguchi, K. Watanabe, G. Gomila, K. S. Novoselov, and A. K. Geim,

“Anomalously low dielectric constant of confined water,” *Science* **360**, 1339–1342 (2018).

⁵¹M. Neumann, “Dipole moment fluctuation formulas in computer simulations of polar systems,” *Mol. Phys.* **50**, 841–858 (1983).

⁵²H. Flyvbjerg and H. G. Petersen, “Error estimates on averages of correlated data,” *J. Chem. Phys.* **91**, 461–466 (1989).